Polymer 49 (2008) 5084–5094

Contents lists available at ScienceDirect

Polymer

journal homepage: www.elsevier.com/locate/polymer

Micellization and phase transition behavior of thermosensitive poly(*N*-isopropylacrylamide)–poly(ε-caprolactone)–poly (*N*-isopropylacrylamide) triblock copolymers

Xian Jun Loh [a,b,c], Yun-Long Wu [a], Wei Tat Joseph Seow [c], Muhammad Nor Irzuan Norimzan [c], Zhong-Xing Zhang [a], Fu-Jian Xu [a,d], En-Tang Kang [d], Koon-Gee Neoh [d], Jun Li [a,b,c,*]

[a] Division of Bioengineering, Faculty of Engineering, National University of Singapore (NUS), 7 Engineering Drive 1, Singapore 117574, Singapore
[b] NUS Graduate School for Integrative Sciences and Engineering (NGS), 28 Medical Drive, Singapore 117456, Singapore
[c] Institute of Materials Research and Engineering, A*STAR (Agency for Science, Technology and Research), 3 Research Link, Singapore 117602, Singapore
[d] Department of Chemical and Biomolecular Engineering, National University of Singapore, Kent Ridge, Singapore 119260, Singapore

ARTICLE INFO

Article history:
Received 23 June 2008
Received in revised form 21 August 2008
Accepted 29 August 2008
Available online 13 September 2008

Keywords:
Triblock block copolymer
Poly(*N*-isopropylacrylamide)
Poly(ε-caprolactone)

ABSTRACT

Thermosensitive triblock copolymers with two hydrophilic poly(*N*-isopropylacrylamide) blocks flanking a central hydrophobic poly(ε-caprolactone) block were synthesized by atom transfer radical polymerization. Core-shell micellization of the triblock copolymers was inferred from the ^{1}H NMR spectra derived in two different solvent environments ($CDCl_3$ and D_2O). The micellar characteristics of these amphiphilic triblock copolymers were studied by pyrene fluorescence techniques, dynamic light scattering and transmission electron microscopy. The critical micelle concentrations of the triblock copolymers were in the range of 4–16 mg/L and the partition coefficients were in the range of 3.10×10^4 to 2.46×10^5. The mean diameters of the micelles, measured by light scattering, were between 90 and 120 nm. The temperature sensitivity of the triblock copolymers was demonstrated by the phase transition of a 250 mg/L aqueous polymer solution at the lower critical solution temperature (LCST). The enthalpy of the phase transition was determined by differential scanning calorimetry. PM3 quantum mechanical calculation method was used to understand the intermolecular interactions between the copolymer and the water molecules. A modular approach was used to simulate the phase transition observed at the LCST.

1. Introduction

Amphiphilic block copolymers have the ability to self-assemble into micelles in the aqueous medium, and have been extensively investigated for their potential application in the fields of nanomedicine and the biomedical areas [1–3]. The micelles have a hydrophobic core and hydrophilic corona which interact with the external aqueous environment. These micelles can aid in the aqueous solubilization of hydrophobic compounds and can act as 'nano-containers' of these compounds. As an example, micelles containing a hydrophobic drug can be injected into the human body. At the onset of injection, it is important that the micelles remain stable and not rupture under the sudden high dilution. Thus, having micelles with a low critical micelle concentration is critical to its application.

Recently, thermosensitive micelles derived from poly(*N*-isopropylacrylamide) (PNIPAAm) have been reported [4–9]. PNIPAAm exhibits a lower critical solution temperature (LCST) of 32–33 °C, being hydrophilic at low temperatures and precipitating above the critical phase transition temperature. Hydrophilic blocks such as poly(ethylene glycol) (PEG) have been linked to PNIPAAm. PEG–PNIPAAm copolymers self-assemble to form micelles upon rising the temperature above the critical phase transition temperature, with PNIPAAm as the hydrophobic core and PEG as the hydrophilic corona [4]. Attaching a hydrophilic component to PNIPAAm also serves to modulate the LCST of the copolymer. For example, attaching PEG with 24 repeating units increases the LCST of the copolymer by 26 °C [5]. On the other hand, block copolymers comprising a hydrophobic segment such as poly(methyl methacrylate) (PMMA), poly(10-undecenoic acid) and poly(oleic acid) and hydrophilic PNIPAAm segments have been reported [6–9]. However, these thermosensitive micelles are non-degradable, raising questions on the elimination of the micelles from the body

* Corresponding author. Division of Bioengineering, Faculty of Engineering, National University of Singapore (NUS), 7 Engineering Drive 1, Singapore 117574, Singapore. Tel.: +65 6516 7273; fax: +65 6872 3069.
E-mail address: bielj@nus.edu.sg (J. Li).

0032-3861/$ – see front matter © 2008 Elsevier Ltd. All rights reserved.
doi:10.1016/j.polymer.2008.08.061

after its use. For this purpose, biodegradable block copolymers such as poly[(*R*)-3-hydroxybutyrate] (PHB) and poly(lactic acid) (PLA) have been copolymerized with poly(ethylene glycol) (PEG) and poly(propylene glycol) (PPG), forming biodegradable thermosensitive micelles and gels which can be eliminated from the body by hydrolytic degradation after its desired period of use [10–13]. The thermo-responsive poly(*N*-isopropylacrylamide-*co*-*N*,*N*-dimethylacrylamide) (PNIPAAm–PDMAAm) segments have been copolymerized with hydrophobic biodegradable segments such as poly(DL-lactic acid) (PDLLA), poly(lactic-*co*-glycolic acid) (PLGA), or poly(ε-caprolactone) (PCL) [14–17]. Biotinylated poly(*N*-isopropylacrylamide-*co*-*N*-(3-dimethylamino propyl)methacrylamide) have been copolymerized with PCL for cell tracking and drug delivery applications [18]. It was demonstrated that these micelles have a slow rate of drug release at temperatures below the critical phase transition temperature but rapidly release encapsulated drug upon heating to above the critical phase transition temperature.

Recently, we synthesized a series of PNIPAAm–PCL–PNIPAAm triblock copolymers by atom transfer radical polymerization (ATRP) for the fabrication of thermo-responsive porous membranes [19]. These triblock copolymers were insoluble in water, having a very long PCL segment with M_n of about 42,000 g/mol which is flanked by short PNIPAAm segments. Recently, another group has synthesized a series of PCL–PNIPAAm–PCL triblock copolymer for drug delivery applications [20]. In this work, we synthesized a series of water-soluble PNIPAAm–PCL–PNIPAAm triblock copolymers with a central short PCL segment with M_n of about 2000 g/mol and extended the PCL block with hydrophilic PNIPAAm blocks of varying lengths on both sides. It would be interesting to study the micelle and phase transition behavior of the copolymers because ATRP allows the controlled synthesis of the block copolymers, yielding well-defined triblock polymeric structures. This makes it possible to study the effect of the hydrophobic/hydrophilic balance of PCL and PNIPAAm without masking the experimental results due to high polydispersity, random or branched polymeric architectures. In this paper, we will present a detailed micelle and phase transition behavior study of the PNIPAAm–PCL–PNIPAAm triblock copolymers.

2. Experimental

2.1. Materials

Dihydroxyl-terminated poly(ε-caprolactone), 2-bromoisobutyryl bromide (98%), *N*-isopropylacrylamide (NIPAAm, >99%), 1,1,4,7,10,10-hexamethyltriethylenetetramine (HMTETA, 99%), copper(I) bromide (CuBr, 99%), triethylamine (>99%) and 1,4-dioxane (>99%) were obtained from Aldrich Chemical Co. of Milwaukee, WI. Purified nitrogen was used in all reactions.

2.2. Synthesis of poly(N-isopropylacrylamide)–poly(ε-caprolactone)–poly(N-isopropylacrylamide) triblock copolymers by atom transfer radical polymerization (ATRP)

The starting ATRP macroinitiator was prepared by a similar process as reported earlier [19]. Typically, 10 g of PCL-diol (–OH end groups = 9 mmol) was dissolved in 80 mL of anhydrous methylene chloride containing 20 mmol of triethylamine in a 250 mL round bottomed flask. The reaction flask was kept in an ice/water bath (temperature = 4 °C). When the PCL-diol had completely dissolved, 10 mmol of 2-bromoisobutyl bromide was added into the flask dropwise through an equalizing funnel. After addition, the reaction was allowed to proceed at room temperature for 24 h. The resulting Br-PCL-Br macroinitiator was precipitated in excess diethylether/methanol (80:20 v/v). The crude product was redissolved in tetrahydrofuran (THF) and re-precipitated in excess diethylether/methanol (80:20 v/v) to remove any residual reactants. This process was repeated another time. The yield of this reaction is about 6.7 g (67%). The Br-PCL-Br macroinitiator for the subsequent ATRP was dried *in vacuo*.

The poly(*N*-isopropylacrylamide)–poly(ε-caprolactone)–poly(*N*-isopropylacrylamide) (PNIPAAm–PCL–PNIPAAm) triblock copolymers were synthesized using a molar feed ratio [NIPAAm (4 g)/[Br-PCL-Br (0.5 g, $M_n = 2160$ g/mol)]/[CuBr (67 mg)]/[HMTETA (213 mg)] of 140:1:2:4. The reaction was performed in a 20 mL flask equipped with a magnetic stirrer. NIPAAm, Br-PCL-Br, and HMTETA were introduced into the flask containing 15 mL of dioxane. After the reactants had dissolved completely, the reaction mixture was degassed by bubbling nitrogen through the reaction mixture for 30 min. CuBr was added into the reaction mixture under nitrogen atmosphere. The reaction mixture was further purged with nitrogen for 10 min. The flask was then sealed and kept under nitrogen atmosphere. The polymerization was allowed to proceed under continuous stirring at 45 °C for 8–24 h. The reaction was stopped by diluting with THF and exposing the reaction mixture to air for 1 h. The catalyst complex was removed by passing the dilute polymer solution through a short aluminium oxide column. A colourless solution was obtained. After removal of THF under reduced pressure, the crude copolymer was redissolved in a minimum amount of THF and precipitated in hexane to remove the unreacted NIPAAm monomer. The obtained precipitate was then dissolved in THF and then re-precipitated in diethylether. The copolymers were then dried *in vacuo* for further studies. The triblock copolymer yields (and the conversion of NIPAAm) from ATRP time of 8, 16, 24 h are 1.41 g (22.8%), 1.84 g (33.5%), 3.12 g (65.5%).

2.3. Molecular characterization

Gel permeation chromatography (GPC) analysis was carried out with a Shimadzu SCL-10A and LC-8A system equipped with two Phenogel 5 μm 50 and 1000 Å columns (size: 300 × 4.6 mm) in series and a Shimadzu RID-10A refractive index detector. THF was used as eluent at a flow rate of 0.30 mL/min at 40 °C. Monodispersed poly(ethylene glycol) standards were used to obtain a calibration curve. The ^{1}H NMR (400 MHz) spectra were recorded on a Bruker AV-400 NMR spectrometer at room temperature. The ^{1}H NMR measurements were carried out with an acquisition time of 3.2 s, a pulse repetition time of 2.0 s, a 30° pulse width, 5208 Hz spectral width, and 32 K data points. Chemical shift was referred to the solvent peaks ($\delta = 7.3$ ppm for $CHCl_3$, $\delta = 4.7$ ppm for HOD).

2.4. Critical micellization concentration (CMC) determination by UV spectroscopy

CMC values were determined by using the dye solubilization method [10]. The hydrophobic dye 1,6-diphenyl-1,3,5-hexatriene (DPH) was dissolved in methanol with a concentration of 0.6 mM. Twenty microliters of this solution was mixed with 2.0 mL of copolymer aqueous solution with concentrations ranging from 3.1×10^{-4} to 10 mg/mL and equilibrated overnight at 4 °C. A UV–vis spectrophotometer was used to obtain the UV–vis spectra in the range of 330–430 nm at 25 °C. The CMC value was determined by the plot of the difference in absorbance at 378 nm and at 400 nm ($A_{378} - A_{400}$) versus logarithmic concentration.

2.5. CMC determination by fluorescence spectroscopy

Steady-state fluorescence spectra were recorded on a Shimadzu RF-5301PC spectrofluorophotometer. Excitation spectra were monitored at $\lambda_{em} = 390$ nm. Fluorescence spectra were monitored at $\lambda_{ex} = 339$ nm. Slit widths for both excitation and emission sides were maintained at 3.0 nm. Sample solutions were prepared by

dissolving a predetermined amount of block copolymer in an aqueous pyrene solution of known concentration, and the solutions were allowed to stand for 1 day for equilibration. The concentration of pyrene was kept at 6.0×10^{-7} M.

2.6. Micelle size measurements

Measurements of micelle size were performed using a Zetasizer Nano ZS (Malvern Instruments, Southborough, MA, USA) with a laser light wavelength of 633 nm at a 173° scattering angle. Micelle solutions were prepared by dissolving the samples in deionised water. The solutions were heated to 40 °C and cooled to 4 °C three times before being kept at 4 °C overnight. The micelle size measurement was performed at 25 °C in triplicate. The micelle solutions (250 mg/L) were passed through a 0.45 μm pore-sized syringe filter before measurements. The deconvolution of the measured correlation curve to an intensity size distribution was accomplished using a non-negative least squares algorithm. The decay rate distributions were transformed to an apparent diffusion coefficient (D). From the diffusion coefficient, the apparent hydrodynamic size of the polymer or micelles can be obtained by the Stokes–Einstein equation. The Z-average hydrodynamic diameters of the particles were given by the instrument. The Z-average size is the intensity weighted mean diameter derived from a cumulants or single-exponential fit of the intensity autocorrelation function.

2.7. Transmission electron microscopy (TEM)

The samples were imaged on a JEOL JEM-2010F FasTEM field emission transmission electron microscope, operated at 100 kV. The samples for TEM were prepared by directly depositing one drop of sample solution onto copper grids, which were coated in advance with supportive Formvar films and carbon (Agar Scientific). The samples were kept in a vacuum oven for 48 h for drying at room temperature before TEM imaging. A drop of the triblock copolymer aqueous solution (0.5 mg/mL) containing 0.1 wt% phosphotungstic acid (PTA) was deposited onto a 200 mesh copper grid coated with carbon. Excessive solution was removed with a Kimwipes delicate wipe. The shape and size of the micelles were directly determined from each transmission electron micrograph.

2.8. Cloud-point temperature determination

Cloud points were measured with a UV–vis spectrophotometer. Aqueous PNIPAAm solutions (250 mg/L) were heated at 2 °C/min while both the transmittance at 500 nm (1 cm path length) and the solution temperature were monitored.

2.9. LCST enthalpy determination

Differential scanning calorimetry (DSC) measurements were performed using a TA Instruments 2920 differential scanning calorimeter equipped with an autocool accessory and calibrated using indium. Samples with a concentration of 10 mg/mL were loaded and sealed in a hematic aluminium pan. The volume of sample used in each case is 10 μL. The following protocol was used for each sample: the first cooling run started from room temperature to 5 °C at 10 °C/min, followed by an isothermal step of 10 min, the heating run started from 5 to 50 °C at 1 °C/min. The enthalpy change associated with the phase transition is obtained from the integrated endothermic peak. LCST was defined as the onset of the endothermic peak [21].

2.10. PM3 quantum mechanical calculation of LCST phenomenon

All calculations were performed using the HyperChem™ Molecular Modeling System (Release 8.0.3). The molecules were first built and geometry optimized by PM3 methods. Hydrogen-bonded complexes were created from the starting molecules with an initial hydrogen bond angle of 180° and hydrogen bond distance of 1.7 A [22]. The parameters for the PM3 setting were as follows: restricted Hartree–Fock calculations were performed with total charge = 0, spin multiplicity = 1, SCF convergence limit was set to 0.0001 with an iteration limit of 50. For the geometry optimization step, the Polak–Ribiere algorithm was utilized. The termination condition was set to an RMS gradient of 0.01 kcal/(Å mol). The enthalpies of association for the complexes were determined at 298 K by determining the difference between the heats of formation for the hydrogen-bonded complexes and the unassociated starting molecules.

3. Results and discussion

3.1. Synthesis of the PNIPAAm–PCL–PNIPAAm triblock copolymers via ATRP

The thermo-responsive PNIPAAm–PCL–PNIPAAm triblock copolymers were prepared according to the reaction sequence shown in Scheme 1. First, the starting dibromo-terminated PCL (Br-PCL-Br) macroinitiator for ATRP was prepared from commercially available PCL-diol by reaction of the terminal hydroxyl end groups of PCL-diol with 2-bromoisobutyryl bromide. The M_n of Br-PCL-Br is about 2.2×10^3 g/mol. These values are comparable to those of the unmodified PCL-diol ($M_n = 2.1 \times 10^3$ g/mol). PNIPAAm–PCL–PNIPAAm triblock copolymer was synthesized via ATRP of NIPAAm from the Br-PCL-Br macroinitiator. The PNIPAAm–PCL–PNIPAAm triblock copolymers were synthesized in dioxane at 45 °C via ATRP of NIPAAm from the Br-PCL-Br macroinitiator units. Triblock copolymers with different contents of the PNIPAAm block were synthesized by varying the polymerization time. A series of PNIPAAm–PCL–PNIPAAm triblock copolymers with different PNIPAAm segment lengths were synthesized. The molecular weights of the copolymers are summarized in Table 1. Controlled ATRP of NIPAAm from Br-PCL-Br can be inferred from the comparable polydispersities with the starting precursor.

The chemical structures of the Br-PCL-Br macroinitiator and the PNIPAAm–PCL–PNIPAAm triblock copolymer were characterized by ^{1}H NMR spectroscopy. The extent of halogenation in the Br-PCL-Br macroinitiator is determined to be about 88% by calculating the area ratio of the peaks at 1.92 ppm (due to the methyl protons of the 2-bromoisobutyryl groups) and 2.2–2.4 ppm (due to the methylene protons adjacent to the carbonyl group of Br-PCL-Br). Fig. 1 shows the ^{1}H NMR spectrum of the NC1 copolymer. The peaks associated with the methyl protons ($\delta = 1.13$ ppm), methylene protons ($\delta = 1.3$–1.8 ppm), methylidyne protons adjacent to the carbonyl group ($\delta = 2.2$–2.4 ppm) and the methylidyne protons adjacent to the amine moiety ($\delta = 4.0$–4.25 ppm) of the PNIPAAm blocks were observed, as reported previously [19]. From NMR, the molecular weights and composition of the block copolymers were calculated and summarized in Table 1.

3.2. Core-shell micelle formation

NMR spectroscopy was used to investigate the effect of solvent on the micelle structure [23–26]. $CDCl_3$ is a good nonselective solvent for PCL and PNIPAAm while water is a good selective solvent for PNIPAAm but poor for PCL. As shown in Fig. 2, in $CDCl_3$, the peaks due to the PCL and PNIPAAm segments were sharp and well defined. In D_2O, PNIPAAm is shown as a sharp peak but PCL peaks are collapsed and broadened. This shows that the molecular motion of PCL is slow in water, indicating a hydrophobic core structure made up of PCL with the hydrophilic PNIPAAm as the

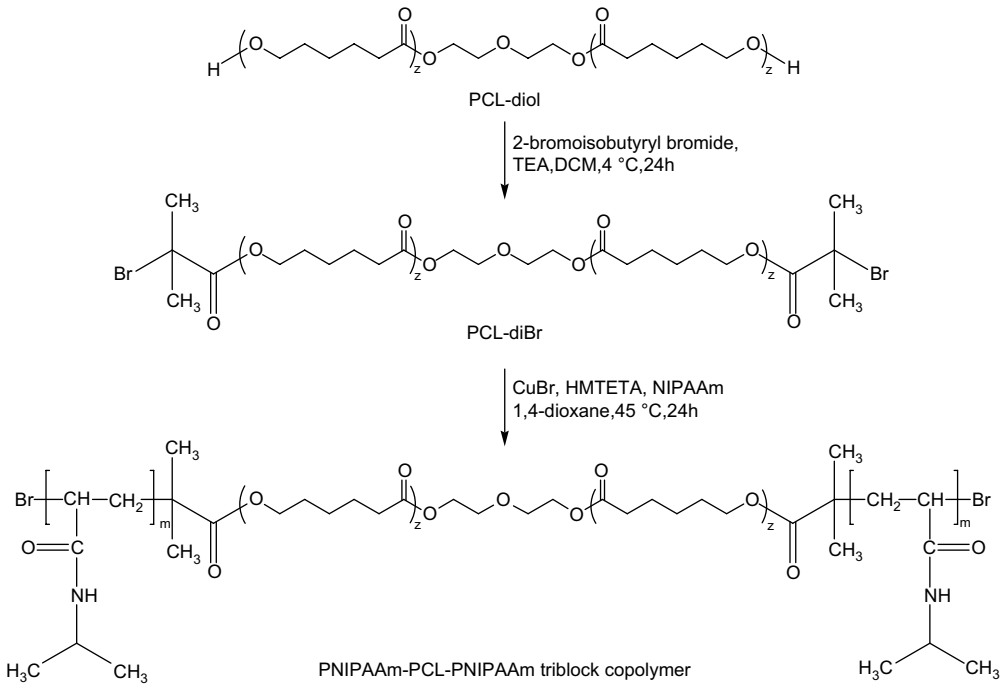

Scheme 1. Synthesis of PNIPAAm–PCL–PNIPAAm triblock copolymers by ATRP.

outer corona structure, confirming the core-corona structure of the micelle [24–26].

3.3. CMC determination

The three PNIPAAm–PCL–PNIPAAm triblock copolymers were soluble in water. The CMC determination was carried out for these three copolymers using the dye solubilization method and fluorescence spectroscopy. For the dye solubilization method, the experiments were conducted by varying the aqueous polymer concentration in the range of 3.1×10^{-4} to 10 mg/mL, while keeping the concentration of DPH constant. DPH shows a higher absorption coefficient in a hydrophobic environment than in water. Thus, with increasing polymer concentration, the absorbances at 344, 358, and 378 nm increased (Fig. 3a). The point where the absorbance suddenly increases corresponds to the concentration at which micelles are formed. When the micelle is formed, DPH partitions preferentially into the hydrophobic core formed in the aqueous solution [23,27,28]. The CMC was determined by extrapolating the absorbance at 378 nm minus the absorbance at 400 nm ($A_{378} - A_{400}$) versus logarithmic concentration (Fig. 3b). The CMC values for the water-soluble copolymers are tabulated in Table 1 and are in the range of 6.9 and 18.2 mg/L. For the DPH solubility experiments, we noticed that there is another slope at around $\log C = 0.3$. There are two reports of this phenomenon when using DPH to determine the micelle properties of amphiphilic copolymers. The reason proposed for this is that the block copolymers are not monodisperse. There is a difference in the hydrophilicities of the copolymers due to the difference in the composition. This will lead to different aggregation behaviors [29,30]. Another reason that could explain this is the fact that there are two distinct events occurring. The primary event is the micelle formation at lower concentrations and the secondary event is the aggregation of the formed micelles at higher concentrations. From our TEM images (see Section 3.5), we noticed the formation of aggregates which are much larger than expected. We propose that the formation of these aggregates could be due to the uneven drying of the micelle solution during the preparation process. This will lead to regions of different polymer concentrations and, therefore, the formation of large aggregates will result from the regions with higher polymer concentration.

Fluorescence probe technique is a powerful tool to study micellar properties of amphiphilic block copolymers [31,32]. When the copolymer concentration in an aqueous solution of pyrene is

Table 1
Molecular characteristics of PNIPAAm–PCL–PNIPAAm triblock copolymers

Copolymer[a]	Copolymer characteristics			Copolymer composition (wt %)[c]				Micelle properties		
	M_n[b] ($\times 10^3$)	M_w/M_n[b]	M_n[c] ($\times 10^3$)	NIPAAm	PCL	CMC (mg/L)[d]	CMC (mg/L)[e]	d[f] (nm)	PD[g]	K_v ($\times 10^{-5}$)[h]
PCL–diBr	2.22	1.69	2.15	–	–	–	–	–	–	–
NC1	5.21	1.68	6.25	65.6	34.4	6.87	3.98	92.7 ± 0.4	0.24	2.46
NC2	6.83	1.36	8.81	75.6	24.4	7.13	6.17	106.3 ± 2.7	0.40	1.90
NC3	17.42	1.54	15.36	86.0	14.0	18.16	15.60	125.3 ± 2.2	0.31	0.31

[a] PNIPAAm–PCL–PNIPAAm triblock copolymers are denoted NC, N for P**N**IPAAm and C for PCL.
[b] Determined by GPC.
[c] Calculated from ^{1}H NMR results.
[d] Determined by 1,6-diphenyl-1,3,5-hexatriene (DPH) dye solubilization method.
[e] Determined by pyrene solubilization method.
[f] Mean diameters by dynamic light scattering from six individual measurements at 25 °C.
[g] Polydispersity factor.
[h] Partition equilibrium coefficient of pyrene in PNIPAAm–PCL–PNIPAAm triblock copolymer.

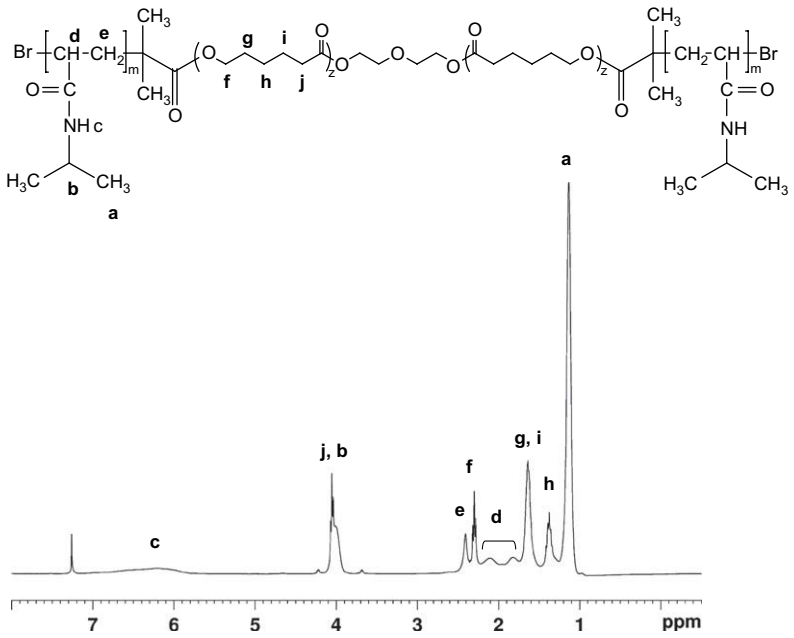

Fig. 1. ^{1}H NMR spectrum of PNIPAAm–PCL–PNIPAAm triblock copolymer in $CDCl_3$ at 25 °C.

increased, both emission and excitation spectra undergo significant changes upon micellization of the block copolymer systems [32]. These changes are caused by the transfer of pyrene molecules from the polar aqueous environment to the hydrophobic micellar cores and are related to the location of the pyrene molecules in the solution. First, the lifetime of the fluorescence decay of the pyrene molecules increase from 200 ns in free aqueous solution to about 350 ns when encapsulated in the hydrophobic micellar core, this is observed together with a corresponding increase in the quantum yield of the fluorescence of pyrene. Second, changes in the fluorescence spectra of pyrene as explained by the Ham effect are observed. The ratio of the intensities of the first and third band of the pyrene fluorescence spectrum (I_1/I_3) decreases when the copolymer concentration increases, indicating a change in the microenvironment of the pyrene molecule. When pyrene is transferred from a polar to a non-polar environment, the symmetry-forbidden (0,0) absorption band is suppressed, which leads to the observed decrease in the intensity ratio. Third, the fluorescence excitation spectrum shows a shift of the low-energy band of the L_a ($S_2 \leftarrow S_0$) from 333 to 338 nm. It has been reported that this (0,0) absorption band change of pyrene is more sensitive to the true onset of aggregation than either lifetime measurements or fluorescence emission changes [33,34]. This change is described in terms of the ratio of the intensities of the first and third bands in the pyrene fluorescence spectrum, I_{338}/I_{333}. Hence, the CMC values of the PNIPAAm–PCL–PNIPAAm triblock copolymers in aqueous solution were determined using the fluorescence excitation spectra of the pyrene probe.

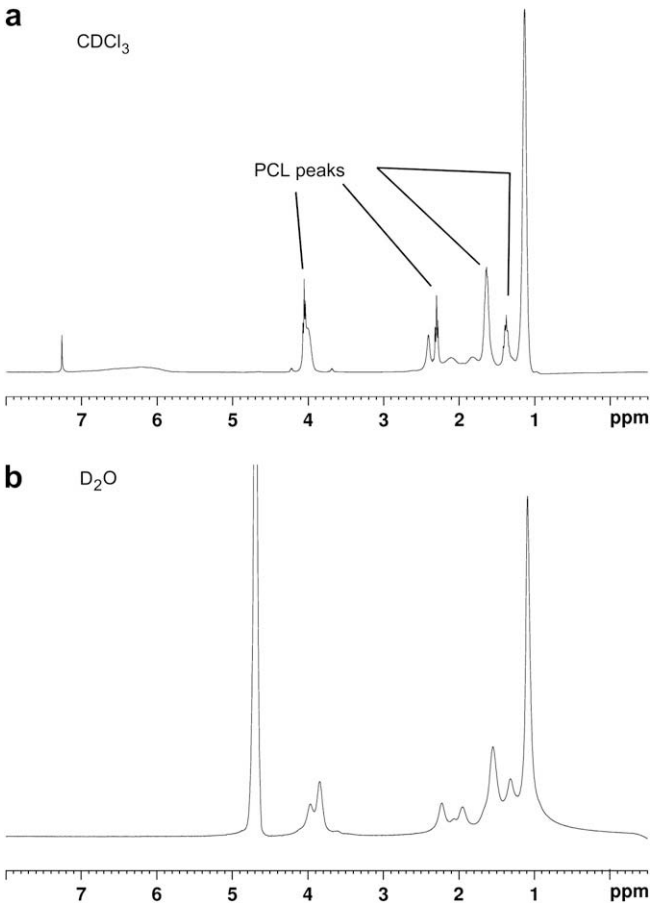

Fig. 2. ^{1}H NMR spectra of NC1 (1 mg/mL) in $CDCl_3$ (a) and D_2O (b) at 25 °C.

The fluorescence spectra of pyrene in water in the presence of increasing concentrations of the triblock copolymers are shown in Fig. 4. The sample is excited at 339 nm and the spectrum is a typical pyrene fluorescence spectrum. Changes in the intensity ratio of the first and the third vibrational bands are observed, similar to previous reports [32,33]. Fig. 5a shows the excitation spectra for pyrene in water at various concentrations of PNIPAAm–PCL–PNIPAAm triblock copolymer. When the copolymer concentration increased, a red shift of the (0,0) absorption band from 333 to 338 nm was observed. Fig. 5b shows the intensity ratio of I_{338}/I_{333} of pyrene excitation spectra as a function of the logarithm of copolymer concentrations for NC1 triblock copolymer. The I_{338}/I_{333} versus log C plots present a sigmoid curve. A negligible change of intensity ratio of I_{338}/I_{333} was observed at low concentration range for each triblock copolymer. With an increase in the copolymer concentration, the intensity ratio exhibited a substantial increase at a certain concentration, reflecting the incorporation of pyrene into the hydrophobic core region of the micelles. Therefore, the CMC values

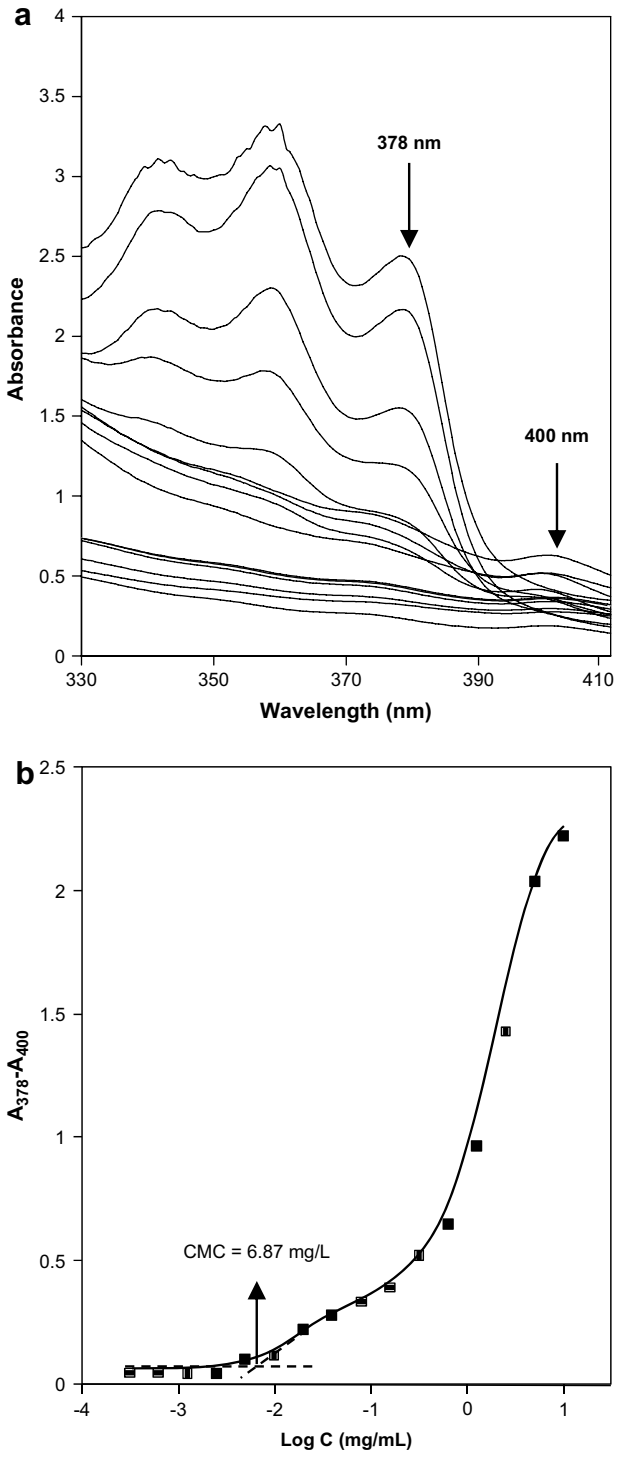

Fig. 3. (a) UV–vis spectra changes of DPH with increasing NC1 copolymer concentration in water at 25 °C. DPH concentration was fixed at 6 mM, and the polymer concentration varied between 3.1×10^{-4} and 10 mg/mL. The increase in the absorbance band at 378 nm indicates the formation of a hydrophobic environment in water. (b) CMC determination by extrapolation of the difference in absorbance at 378 and 400 nm.

were determined form the crossover point at the low concentration range in Fig. 5b. The CMC values determined by fluorescence spectroscopy for the water-soluble copolymers are tabulated in Table 1 and are in the range of 4.0 and 15.6 mg/L. The very low CMC values for PNIPAAm–PCL–PNIPAAm triblock copolymers, indicate a very strong tendency of the triblock copolymers toward formation

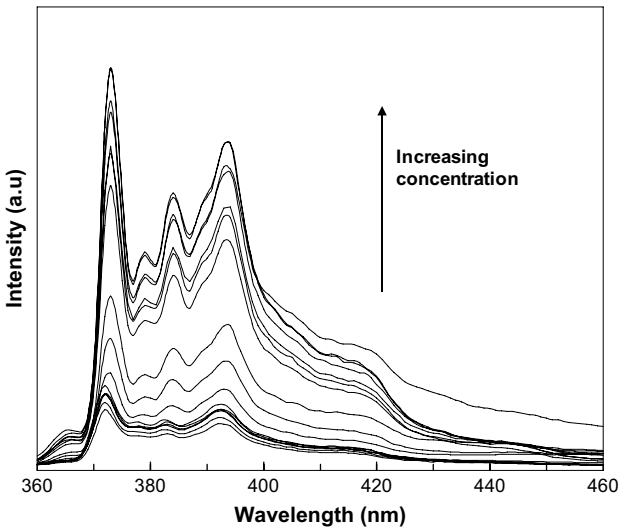

Fig. 4. Fluorescence spectra of pyrene (6×10^{-7} M) in water in the presence of increasing concentration of the triblock copolymer sample, NC1.

of micelles in aqueous solution. The CMC values of the triblock copolymers were observed to increase with an increase in the PNIPAAm segment length, due to the increased hydrophilicity of this segment. Generally, PNIPAAm-based micelles have CMC values within this decade, the values reported were 10 mg/L (star block copolymer based on PMMA and PNIPAAm), 20 mg/L (block copolymer based on poly(undecylenic acid) and PNIPAAm) and 13 mg/L (block copolymer based on poly(oleic acid) and PNIPAAm) [6,7,9]. When compared with the CMC values obtained with the DPH dye solubilization method, the CMC values obtained in this manner were slightly lower but showed reasonable agreement.

3.4. Partitioning of pyrene in micelles

The hydrophobicity of the PCL micellar core can be estimated by determining the partition equilibrium coefficient, K_v of pyrene, in the aqueous PNIPAAm–PCL–PNIPAAm triblock copolymer solutions. The calculations were performed as reported previously [32,35–37]. This method calculates the partition equilibrium based on the assumption of a simple equilibrium distribution between the micellar phase and the water phase. The ratio of the pyrene concentration in the micellar phase to the water phase ($[Py]_m/[Py]_w$) can be correlated to the ratio of volume of each phase and expressed as follows.

$$([Py]_m/[Py]_w) = K_v V_m/V_w \quad (1)$$

This can be rewritten as

$$([Py]_m/[Py]_w) = K_v x(c - \mathrm{CMC})/1000\rho \quad (2)$$

where x is the weight fraction of the PCL block in the triblock copolymer, c is the concentration of the triblock copolymer, and ρ is the density of the PCL core of the micelles, which is assumed to be the bulk density of PCL (1.146 g/cm^3). In the intermediate range of the polymer concentrations with substantial increases in the intensity ratios (I_{338}/I_{333}), ($[Py]_m/[Py]_w$) can be written as

$$([Py]_m/[Py]_w) = (F - F_{min})/(F_{max} - F) \quad (3)$$

where F_{min} and F_{max} correspond to the average magnitude of the intensity ratio (I_{338}/I_{333}) in the constant region in the low and high concentration ranges in Fig. 5, respectively. F is the intensity ratio

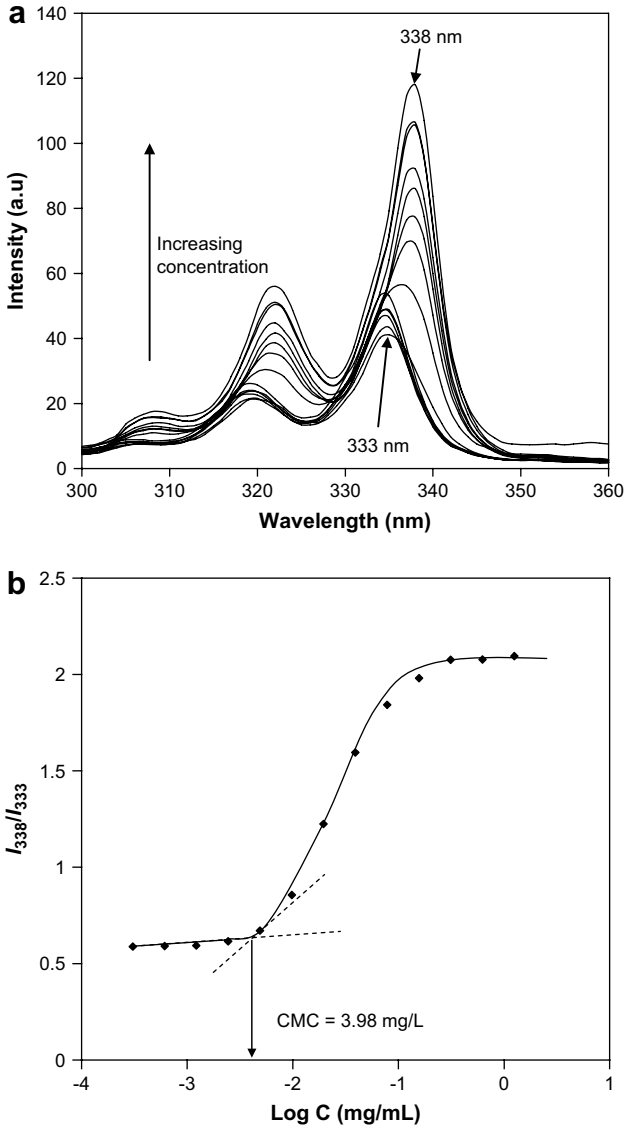

Fig. 5. (a) Steady-state fluorescence excitation spectra monitored at 390 nm for the pyrene probe in an aqueous solution of NC1 copolymer of various concentrations in water at 25 °C. The concentration of pyrene is 6.0×10^{-7} M. (b) Plots of the I_{338}/I_{333} ratio of pyrene excitation spectra in water as a function of NC1 triblock copolymer concentration at 25 °C.

(I_{338}/I_{333}) in the intermediate concentration range of the triblock copolymers. Combining Eqs. (2) and (3) yields

$$(F - F_{\min})/(F_{\max} - F) = K_v x(c - \mathrm{CMC})/1000\rho \quad (4)$$

K_v values for pyrene were obtained by plotting a graph of $(F - F_{\min})/(F_{\max} - F)$ versus the concentration of the PNIPAAm–PCL–PNIPAAm triblock copolymer solutions, as shown in Fig. 6. The K_v values are summarized in Table 1. The values ranged from 3.10×10^4 to 2.46×10^5 for the triblock copolymers. As the length of the PNIPAAm chains increased, the K_v values decreased, suggesting that the hydrophobicities of the micellar core decreased. This is related to the hydrophilic/hydrophobic balance in the triblock copolymer, which consequently affects the micelle packing ability of the copolymer. Previously, K_v values of 3.0×10^4 to 3.3×10^5 have been reported for amphiphilic poly[bis(2,2,2-trifluoroethoxy)phosphazene]/poly(propylene glycol) triblock copolymers and K_v values of 1.79×10^5 to 5.88×10^5 have been reported for copolymers of poly(2-ethyl-2-oxazoline)–poly(ε-caprolactone) and poly(2-ethyl-2-oxazoline)-poly(L-lactide) [36,37].

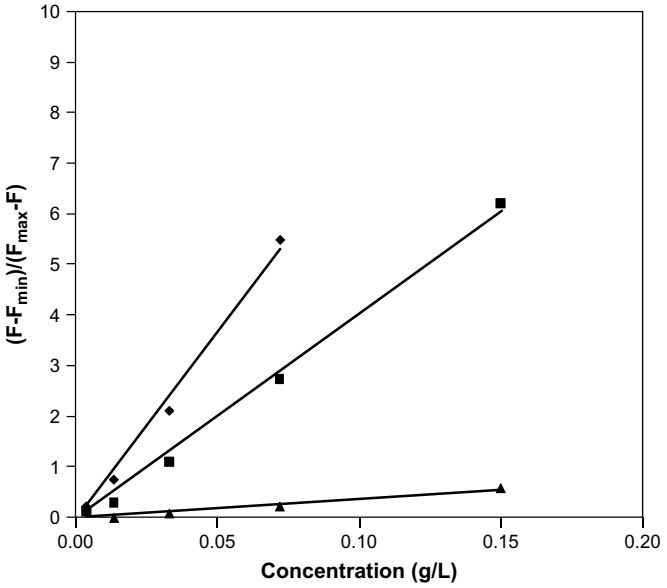

Fig. 6. Plots of $(F - F_{\min})/(F_{\max} - F)$ versus concentration of PNIPAAm–PCL–PNIPAAm triblock copolymers, NC1 (◆), NC2 (■) and NC3 (▲) in water at 25 °C.

3.5. Size of micelles

The size of a micelle is a significant determinant of its application. For example, it has been mentioned that the small size of micelles (<200 nm) make them suitable carriers of drugs as they are less susceptible to uptake by the reticuloendothelial system [38,39]. The uptake characteristics of any drug encapsulated in the micelle will be affected by the morphology and the size of the particles. The morphology and size distribution of the copolymer micelles were investigated by TEM observation and dynamic light scattering (DLS), respectively, (Fig. 7). From TEM micrographs, spherical micelles were dispersed as individual nanoparticles. We observed particles of different sizes, most of them were small particles and there were some larger particles. The diameters of the smaller particles were about 50–100 nm. The inset of Fig. 7a shows the magnified image of a particle. From the image, a dense dark core and a less dense corona are observed. This is due to the action of the staining agent, phosphotungstic acid, which stains the hydrophobic core to a greater extent. From DLS measurements, these diameters of the micelles range from 90 to 120 nm, increasing as the PNIPAAm segment becomes longer. The polydispersity of the micelle size ranged from 0.2 to 0.4. Further, it appears from the TEM micrographs that the micelles have a very broad distribution of the different sizes. This is clearly different from the observation from DLS. This has to be related to the fact that DLS measures the hydrodynamic diameter of the micelles in an aqueous environment whereas the TEM micrographs show the dehydrated solid state of the micelles. Sample preparation steps, such as the drying of the micelle solution, could lead to an uneven distribution of micelle concentration on the copper grid. In regions of high polymer concentration, there could be micelle aggregation, brought about by either PNIPAAm chain entanglements or hydrophobic association of the micelles. This could lead to the formation of a more polydisperse distribution of particles for the TEM sample compared to the DLS sample. The smaller diameter from the TEM study can be attributed to the dehydration and subsequent collapse of the PNIPAAm chain end when the sample is dried, this corroborates with the reports made in other papers [6–9,18]. Aggregated particles were also observed in the TEM images of these papers, indicating the tendency for PNIPAAm-based micelles to aggregate [6–8,20].

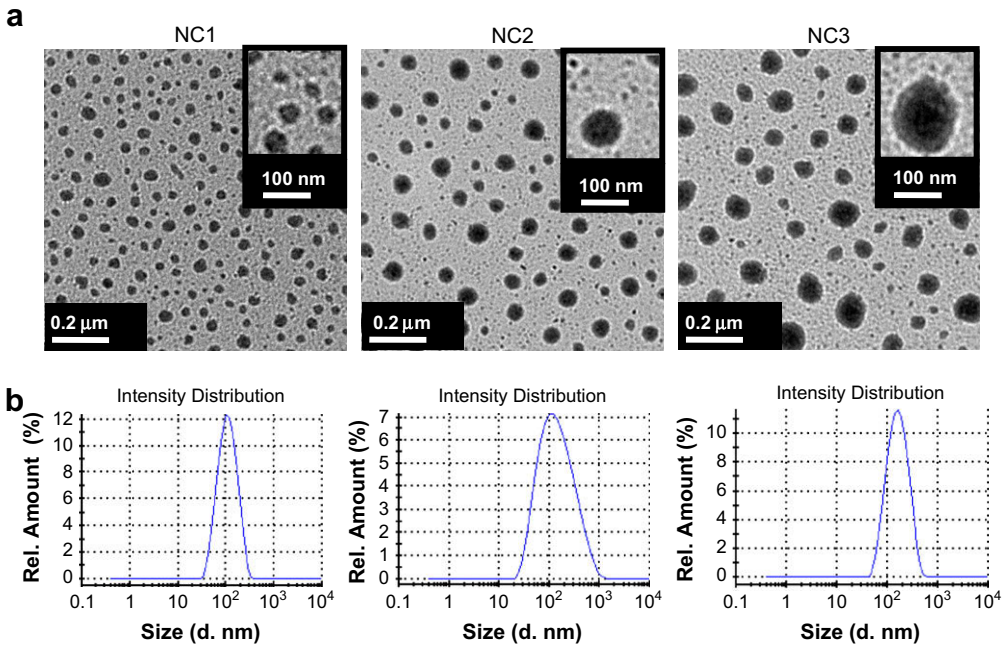

Fig. 7. (a) TEM micrographs of the PNIPAAm–PCL–PNIPAAm triblock copolymer micelles. (b) Particle size distribution of the PNIPAAm–PCL–PNIPAAm triblock copolymer micelles (solution concentration = 250 mg/L).

3.6. Solution properties at LCST

The PNIPAAm–PCL–PNIPAAm triblock copolymer micelles were water soluble at 25 °C with a hydrophobic PCL core and hydrophillic PNIPAAm corona. When the temperature of the solution is increased, the hydrophobicity of PNIPAAm increases and PNIPAAm chains in the micelle corona collapse. The increased hydrophobicity of the micelles will lead to micelle aggregation, leading to the formation of larger particles. The thermosensitivity of the PNIPAAm–PCL–PNIPAAm triblock copolymer micelles was demonstrated by observing the change in the optical absorbance of a micellar solution as a function of temperature. PNIPAAm exhibits a temperature sensitive phase transition in the temperature range of 32–33 °C. This temperature is known as the cloud-point temperature and has been used to determine the lower critical solution temperature (LCST) of PNIPAAm. The cloud-point temperatures of the copolymers are presented in Table 2. At temperatures below the cloud-point temperature, PNIPAAm is a hydrophilic water-soluble polymer and we observe a clear solution. Above this temperature, PNIPAAm becomes hydrophobic and precipitates out of the aqueous solution. In this paper, the cloud-point temperature is defined as the temperature exhibiting a 50% decrease in optical transmittance of an aqueous copolymer solution (250 mg/L) at 500 nm (Fig. 8). NC1 copolymer (M_n (PNIPAAm block) ~4000 g/mol) exhibits a cloud-point temperature of 30.6 °C. Xia et al. have reported a cloud-point temperature of 38.9 °C for pure PNIPAAm with M_n of 5000 g/mol [40]. NC2 copolymer (M_n (PNIPAAm block) ~6500 g/mol) exhibits a cloud-point temperature of 31.8 °C, the corresponding PNIPAAm, with M_n of 7000 g/mol has a cloud-point temperature of 36.3 °C. NC3 copolymer (M_n (PNIPAAm block) ~13000 g/mol) exhibits a cloud-point temperature of 32.7 °C, the corresponding PNIPAAm, with M_n of 13,200 g/mol has a cloud-point temperature of 35.5 °C. It can be seen from the results that the incorporation of the hydrophobic PCL lowers the cloud-point temperature compared to the PNIPAAm homopolymer. While in Xia's work, the cloud-point temperatures decrease to a constant value as the molecular weight increases, the results of the cloud-point temperatures are expected to increase to a constant value with increasing PNIPAAm chain length. The changes observed in this case are due to the changes in the polymer/solvent interactions arising from the change in the

Table 2
Cloud-point properties of aqueous solutions of PNIPAAm–PCL–PNIPAAm triblock copolymers

Copolymer	LCST[a] (°C)	LCST[b] (°C)	ΔH^c (J/g)	ΔH^d (kJ/mol)
NC1	30.6	29.1	14.1	1.6
NC2	31.8	29.4	28.9	3.3
NC3	32.7	29.9	57.4	6.5

[a] Determined from turbidmetry measurements.
[b] Determined from DSC.
[c] Enthalpy of endotherm (J/g of PNIPAAm).
[d] Enthalpy of endotherm (kJ/mole of monomer repeating unit of PNIPAAm).

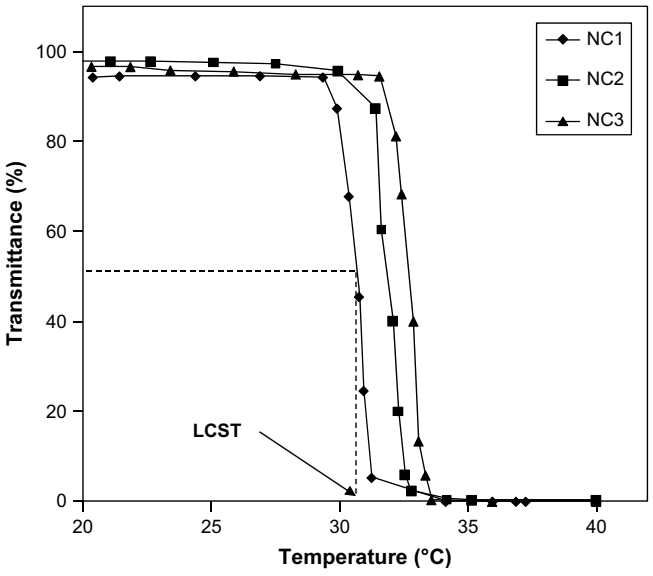

Fig. 8. Cloud-point curves for the PNIPAAm–PCL–PNIPAAm triblock copolymers (250 mg/L) in water.

hydrophilic/hydrophobic balance of the copolymers. For the PNIPAAm–PCL–PNIPAAm triblock copolymers, the copolymers become more hydrophilic as the PNIPAAm segments become longer, leading to the observed increase in the cloud-point temperature.

3.7. Enthalpy of phase transition

DSC can also be used to determine the phase separation temperature of these polymers [41–43]. The precipitation phenomenon was observed in these systems and results in the observation of an endothermic peak in the DSC thermograms (Fig. 9). This is due to a sudden conformational change where the hydrated random coils collapse into globular particles. In the hydrated state, the water molecules are bound by hydrogen bonds to the amide groups of PNIPAAm. As the temperature is raised, the polymer–solvent interaction becomes weaker and the hydrogen bonds eventually break at the lower critical transition temperature. The breaking of the hydrogen bond results in the endothermic heat of transition as observed in the DSC thermogram [41–43]. For the PNIPAAm–PCL–PNIPAAm aqueous solutions, the enthalpy of separation was between 9.25 and 49.4 J/g of polymer. This corresponds to 1.59–6.49 kJ/mol of NIPAAm monomer repeating unit. Schild [41] and Fujishige [44] have reported enthalpy changes in the range of 4.8–6.2 kJ/mol of NIPAAm monomer repeating unit, this corresponds to the loss of approximately one hydrogen bond per NIPAAm repeating unit [42]. The copolymers with a longer PNIPAAm chain showed a greater enthalpy change. Similar observations have been made by Schild and Tirrell [41]. For the copolymers, the LCST determination is determined by the onset of the endotherm transition. The LCST values obtained from DSC are slightly lower than that obtained from transmittance studies, consistent with the study reported by Boutris et al. [42]. This is due to the more sensitive nature of the DSC study compared to the transmittance study toward the phase transition of the aqueous polymer solution. DSC detects the onset of the phase transition, which is the disruption of the hydrogen bonds between the polymer and the solvent molecules. On the other hand, the transmittance changes can only be observed when the polymer undergoes the second stage of phase transition where the hydrated coils collapse into globules [42].

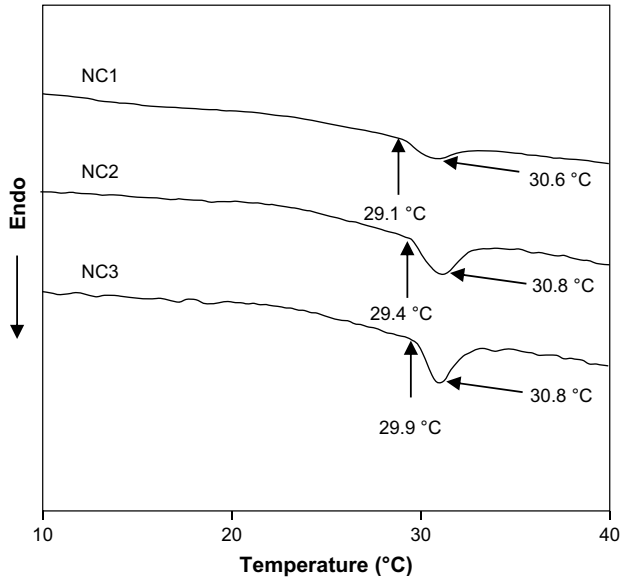

Fig. 9. DSC curves of the aqueous solutions of PNIPAAm–PCL–PNIPAAm triblock copolymers (10 mg/mL).

3.8. PM3 quantum mechanical calculations of phase transition enthalpy

In order to better understand the water–polymer interactions, the PM3 semi-empirical quantum mechanical method was utilized. This method offers a reasonably accurate simulation of the behavior of the polymer molecules in solution and does not require extensive computing power. This semi-empirical method has been demonstrated to describe the intermolecular hydrogen bonding in small polar molecules [22,45]. Attempting to simulate the LCST behavior of the macromolecules is a daunting task. This problem can be simplified by investigating small models which possess the interactions present in the macromolecules [45]. For simplicity of calculations, model systems involving a monomer of NIPAAm ($NIPAAm_1$) or a trimer of NIPAAm ($NIPAAm_3$) were built and geometry optimized. The enthalpies of association were obtained from the difference of the ΔH_f of the hydrogen-bonded complexes and the sums of the ΔH_f for the monomers (Table 3). With $NIPAAm_1$, the strength of the hydrogen bond associated with the water molecule and the carbonyl oxygen of NIPAAm was calculated to be 16.8 kJ/mol of NIPAAm monomer repeating unit. On the other hand, the strength of the hydrogen bond associated with the water molecule and the amide proton of NIPAAm was calculated to be 6.7 kJ/mol of NIPAAm monomer repeating unit. With $NIPAAm_3$, the strength of the hydrogen bond associated with the water molecule and the carbonyl oxygen of NIPAAm was calculated to be 7.9 kJ/mol of NIPAAm monomer repeating unit. On the other hand, the strength of the hydrogen bond associated with the water molecule and the amide proton of NIPAAm was calculated to be 4.8 kJ/mol of NIPAAm monomer repeating unit. The higher values obtained with $NIPAAm_1$ could be related to its greater degree of hydration (1–2 H_2O molecule per monomer unit) compared with $NIPAAm_3$ (0.33–0.66 H_2O molecule per monomer unit). Previously, Tamai et al. have calculated the hydrogen bond energies of PNIPAAm [46]. The strength of the hydrogen bond between the carbonyl oxygen and the water molecule was 24.7 kJ/mol and the strength of the hydrogen bond between the amide proton and the water molecule was 29.7 kJ/mol. The difference in the relative strength of the hydrogen bond can be attributed to the different calculation techniques employed. Tamai et al. calculated their values based on molecular mechanics (AMBER/OPLS force field). Nonetheless, the values calculated in this study are important for our purpose of comparison. Our calculated values agree fairly well with Tamai's

Table 3
Calculated PM3 heats of formation of water clusters and NIPAAm derivatives

Molecule	$\Delta H_{f^\circ,\ 298K}$ (kJ/mol)	Enthalpy of association for complex relative to separated molecular species (kJ/mol)
$NIPAAm_1$	−289.0	–
$NIPAAm_3$	−769.0	–
H_2O	−223.7	–
$(H_2O)_2$	−462.0	−14.6
$(H_2O)_3$	−708.5	−37.5
$(H_2O)_4$	−960.8	−66.1
$NIPAAm_1$–H_2O	−529.5	−16.8
$NIPAAm_1$–$2H_2O$	−759.9	−23.5
$NIPAAm_3$–H_2O	−1016.4	−23.7
$NIPAAm_3$–$2H_2O$	−1254.5	−38.2
($NIPAAm_1$–H_2O) + ($NIPAAm_1$–H_2O)	−1075.8	−50.5
($NIPAAm_1$–H_2O) + ($NIPAAm_1$–$2H_2O$)	−1324.5	−75.5
($NIPAAm_1$–$2H_2O$) + ($NIPAAm_1$–$2H_2O$)	−1569.2	−96.5
($NIPAAm_3$–H_2O) + ($NIPAAm_3$–H_2O)	−2068.1	−82.7
($NIPAAm_3$–H_2O) + ($NIPAAm_3$–$2H_2O$)	−2315.8	−106.7
($NIPAAm_3$–$2H_2O$) + ($NIPAAm_3$–$2H_2O$)	−2558.7	−125.9
$NIPAAm_1$–$NIPAAm_1$	−599.8	−21.8
$NIPAAm_3$–$NIPAAm_3$	−1577.5	−39.4

values, especially for the hydrogen bond between the water molecule and the carbonyl oxygen.

The next area of consideration is in the calculation of the enthalpy of the phase transition of the copolymers in aqueous solution. There have been many suggested mechanisms for the phase transition of the PNIPAAm aqueous solutions. The phase transition has been shown to consist of at least two different processes by Cho et al. [47]. That paper proposed a transition model comprising three processes, first, the water cages around the hydrophobic part of PNIPAAm rearranges to bulk water. Second, the water bound to the hydrophilic amide region of PNIPAAm rearranges to bulk water. Finally, the PNIPAAm chains associate, either by van der Waals interactions or hydrogen bonding. In our modular-approach model of phase transition, we started with the hydrogen complexes of NIPAAm and water, denoted by ($NIPAAm_x$–xH_2O), as the initial reactants. The products of the reaction are the associated NIPAAm molecules, denoted by ($NIPAAm_x$–$NIPAAm_x$), and the water clusters, denoted by $(H_2O)_x$. In this case, the heat of formation of the associated $NIPAAm_x$–xH_2O and $NIPAAm_x$–$NIPAAm_x$ species as well as the water clusters, $(H_2O)_x$ was calculated. The enthalpies of association were obtained by the difference in the heat of formation of the complexes from the separated molecular species. The results are summarized in Table 3. From these results, it is clear that $NIPAAm_3$ provides a better picture of the phase transition. Comparing the calculated values obtained with $NIPAAm_1$ and $NIPAAm_3$, it appears that with a higher degree of hydration, the enthalpy change associated with the phase transition is greater. When compared with the experimental DSC values, it appears that the more hydrophobic triblock copolymer (NC1) is less hydrated than the copolymer with longer NIPAAm chains (NC3). Furthermore, the calculations reveal that the formation of bulk hydrogen-bonded water clusters play an important role in stabilizing the entire system. The water clusters were more stable compared with the separated water molecules (Table 3). The enthalpy values obtained experimentally agree very well with the calculated values. This suggests that the PM3 method of calculation is feasible for predicting enthalpy change related to the phase transition of PNIPAAm. From the obtained molecular structures, it can be seen that the water molecules form hydrogen bonds with the two individual NIPAAm chains and act as a bridge, linking the two molecules together (Fig. 10). This link also serves to stabilize the supramolecular structure and maintain the NIPAAm molecule in a hydrated state. From the figure, it can be seen that the $(NIPAAm_3–2H_2O) + (NIPAAm_3–2H_2O)$ species is stabilized by two water 'bridges'. This extra stabilization effect explains the calculation result that shows that the simulated reaction **6** (having two water bridges) has a less endothermic enthalpy compared with either **4** or **5** (having one water bridge) (Table 4). Comparing the molecular structures in Fig. 10, as the molecules become more hydrated, the cavity between the two NIPAAm species becomes larger. Looking at Fig. 10(b), the two NIPAAm molecules are very close together whereas in Fig. 10(d), the molecules are spaced further apart. The spacing of the NIPAAm molecules could influence the ease of the phase transition. This could be a contributing reason for the lower LCST observed when PCL is incorporated into the triblock copolymer. PCL increases the hydrophobicity of the copolymer and subsequently, the triblock copolymer is less hydrated in the aqueous environment. In such a situation, the NIPAAm blocks are spaced more closely together and this could enhance the NIPAAm–NIPAAm association.

From the molecular simulation, two key points can be observed. First, as the degree of hydration increases, the enthalpy change associated with the phase transition becomes more endothermic. The trend observed experimentally is as follows: NC3 (most endothermic) > NC2 > NC1 (least endothermic). From our model, this is primarily related to the total number of hydrogen bonds

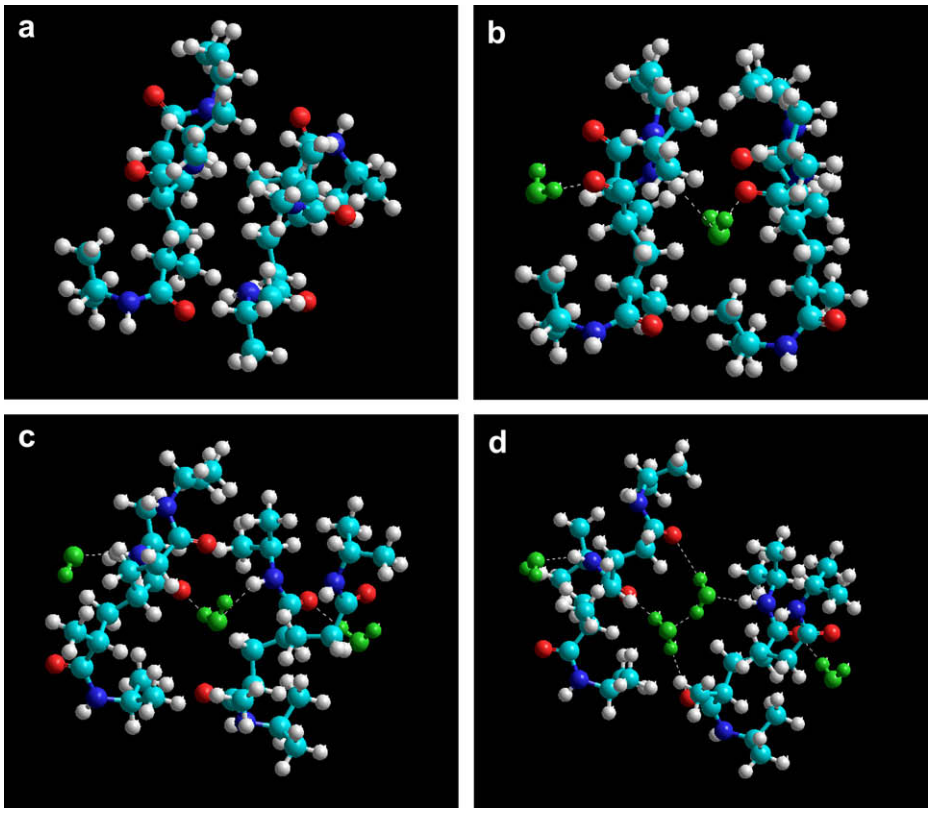

Fig. 10. Molecular structures of the $NIPAAm_3$ and water complexes (a) $NIPAAm_3$–$NIPAAm_3$, (b) $(NIPAAm_3–H_2O) + (NIPAAm_3–H_2O)$, (c) $(NIPAAm_3–H_2O) + (NIPAAm_3–2H_2O)$, (d) $(NIPAAm_3–2H_2O) + (NIPAAm_3–2H_2O)$. (Water molecules are highlighted in green. Hydrogen bonds are indicated by the dotted lines).

Table 4
Simulated enthalpy of phase transition

Reaction number	Simulated system	Enthalpy of association for complex relative to separated molecular species (kJ/mol)[a]
1	$(NIPAAm_1–H_2O) + (NIPAAm_1–H_2O) \rightarrow NIPAAm_1–NIPAAm_1 + (H_2O)_2$	7.0
2	$(NIPAAm_1–H_2O) + (NIPAAm_1–2H_2O) \rightarrow NIPAAm_1–NIPAAm_1 + (H_2O)_3$	8.1
3	$(NIPAAm_1–2H_2O) + (NIPAAm_1–2H_2O) \rightarrow NIPAAm_1–NIPAAm_1 + (H_2O)_4$	4.3
4	$(NIPAAm_3–H_2O) + (NIPAAm_3–H_2O) \rightarrow NIPAAm_3–NIPAAm_3 + (H_2O)_2$	4.8
5	$(NIPAAm_3–H_2O) + (NIPAAm_3–2H_2O) \rightarrow NIPAAm_3–NIPAAm_3 + (H_2O)_3$	5.0
6	$(NIPAAm_3–2H_2O) + (NIPAAm_3–2H_2O) \rightarrow NIPAAm_3–NIPAAm_3 + (H_2O)_4$	3.4

[a] Enthalpy of association (kJ/mole) of monomer repeating unit of PNIPAAm.

formed between the water molecules and the monomer unit, which corresponds to the degree of hydration. With a greater degree of hydration, more energy has to be supplied to the system to break the hydrogen bonds. Second, the hydrophilic and hydrophobic balance of the copolymer are very important in determining the degree of hydration and consequently the micelle packing ability of the copolymers in aqueous solution. For example, NC3 has the lowest K_v value of all three copolymers (demonstrating the lowest micellar core hydrophobicity) but has the most endothermic heat of phase transition (due to its greatest degree of hydration).

4. Conclusions

Thermosensitive triblock copolymers having two hydrophilic poly(*N*-isopropylacrylamide) blocks linked to a central hydrophobic poly(ε-caprolactone) block were synthesized by atom transfer radical polymerization. The triblock copolymers formed micelles with a hydrophobic PCL core and a hydrophilic PNIPAAm shell as inferred from the ^{1}H NMR spectra derived in two different environments ($CDCl_3$ and D_2O). The CMC of the triblock copolymers was very low and have great stability under high dilution conditions. The hydrophobicity of the micellar cores was estimated by measuring the partition equilibrium constant of pyrene in the micellar solution of the triblock copolymers. The hydrophobicity of the micellar core could be controlled by adjusting the composition of the copolymer. The mean diameters of the micelles, measured by light scattering, were between 90 and 120 nm. Some large aggregates could be observed in the TEM images. This could be due to the sample preparation process. The temperature sensitivity of the triblock copolymers was studied by the turbimetry method and by DSC. PM3 quantum mechanical calculation method was used to provide additional insights on the intermolecular interactions between the polymer and the water molecules. The enthalpy values obtained from the simulated phase transition agree very well with the experimentally obtained data. The exciting potential for this copolymer lies in the tunability of these characteristics by varying its composition, thus allowing it to be designed for specific drug delivery applications in the future.

Acknowledgements

We acknowledge the financial support from National University of Singapore and Institute of Materials Research and Engineering. X.J. Loh would like to thank the A*STAR Graduate Scholarship.

Appendix. Supporting information

Supporting information associated with this article can be found in the online version, at doi: 10.1016/j.polymer.2008.08.061.

References

[1] Torchilin VP. J Controlled Release 2001;73:137–72.
[2] Kwon GS, Kataoka K. Adv Drug Deliv Rev 1995;16:295–309.
[3] Li J, Li X, Ni X, Leong KW. Macromolecules 2003;36:2661–7.
[4] Motokawa R, Morishita K, Koizumi S, Nakahira T, Annaka M. Macromolecules 2005;38:5748–60.
[5] Kim YC, Kil DS, Kim JC. J Appl Polym Sci 2006;101:1833–41.
[6] Wei H, Zhang XZ, Cheng C, Cheng SX, Zhuo RX. Biomaterials 2007;28:99–107.
[7] Li YY, Zhang XZ, Cheng H, Kim GC, Cheng SX, Zhuo RX. Biomacromolecules 2006;7:2956–60.
[8] Wei H, Zhang XZ, Cheng H, Chen WQ, Cheng SX, Zhuo RX. J Controlled Release 2006;116:266–74.
[9] Li YY, Zhang XZ, Kim GC, Cheng H, Cheng SX, Zhuo RX. Small 2006;2:917–23.
[10] Loh XJ, Goh SH, Li J. Biomacromolecules 2007;8:585–93.
[11] Loh XJ, Li J. Expert Opin Ther Pat 2007;17:965–77.
[12] Loh XJ, Goh SH, Li J. Biomaterials 2007;28:4113–23.
[13] Loh XJ, Tan YX, Li Z, Teo LS, Goh SH, Li J. Biomaterials 2008;29:2164–72.
[14] Kohori F, Sakai K, Aoyagi T, Yokoyama M, Yamato M, Sakurai Y, et al. Colloids Surf B 1999;16:195–205.
[15] Liu SQ, Tong YW, Yang YY. Biomaterials 2005;26:5064–74.
[16] Liu SQ, Tong YW, Yang YY. Mol Biosyst 2005;1:158–65.
[17] Nakayama M, Okano T, Miyazaki T, Kohori F, Sakai K, Yokoyama M. J Controlled Release 2006;115:46–56.
[18] Li YY, Zhang XZ, Cheng H, Zhu JL, Li UN, Cheng SX, et al. Nanotechnology 2007;18:505101.
[19] Xu FJ, Li J, Yuan SJ, Zhang ZX, Kang ET, Neoh KG. Biomacromolecules 2008;9:331–9.
[20] Chang C, Wei H, Quan CY, Li YY, Liu J, Wang ZC, et al. J Polym Sci Part A Polym Chem 2008;46:3048–57.
[21] Otake K, Inomata H, Konno M, Saito S. Macromolecules 1990;23:283–9.
[22] Jurema MW, Shields GC. J Comput Chem 1993;14:89–104.
[23] Jeong B, Bae YH, Kim SW. Macromolecules 1999;32:7064–9.
[24] Jeong B, Bae YH, Kim SW. Colloids Surf B 1999;16:185–93.
[25] Jeong B, Windisch Jr CF, Park MJ, Sohn MJ, Gutowska A, Char K. J Phys Chem B 2003;107:10032–9.
[26] Lee BH, Lee YM, Sohn YS, Song SC. Macromolecules 2002;35:3876–9.
[27] Hwang MJ, Suh JM, Bae YH, Kim SW, Jeong B. Biomacromolecules 2005;6:885–90.
[28] Alexandridis P, Holzwarth JF, Hatton TA. Macromolecules 1994;27:2414–25.
[29] Zhou Z, Chu B. Macromolecules 1988;21:2548–54.
[30] Gaisford S, Beezer AE, Mitchell JC, Bell PC, Fakorede F, Finnie JK, et al. Int J Pharm 1998;174:39–46.
[31] Astafieva I, Zhong XF, Eisenberg A. Macromolecules 1993;26:7339–52.
[32] Wilhelm M, Zhao C, Wang Y, Xu R, Winnik MA, Mura JL, et al. Macromolecules 1991;24:1033–40.
[33] Li J, Ni XP, Li X, Tan NK, Lim CT, Ramakrishna S, et al. Langmuir 2005;21:8681–5.
[34] Li X, Mya KY, Ni X, He C, Leong KW, Li J. J Phys Chem B 2006;110:5920–6.
[35] Chang Y, Lee SC, Him KT, Him C, Reeves SD, Allcock HR. Macromolecules 2001;34:269–74.
[36] Allcock HR, Cho SY, Steely LB. Macromolecules 2006;39:8334–8.
[37] Lee SC, Chang YK, Yoon JS, Kim CH, Kwon IC, Kim YH, et al. Macromolecules 1999;32:1847–52.
[38] Kataoka K, Harada A, Nagasaki Y. Adv Drug Deliv Rev 2001;47:113–31.
[39] Jones MC, Leroux JC. Eur J Pharm Biopharm 1999;48:101–11.
[40] Xia Y, Yin XC, Burke NAD, Stover HDH. Macromolecules 2005;38:5937–43.
[41] Schild HG, Tirrell DA. J Phys Chem 1990;94:4352–6.
[42] Boutris C, Chatzi EG, Kiparissides C. Polymer 1997;38:2567–70.
[43] Idziak I, Avoce D, Lessard D, Gravel D, Zhu XX. Macromolecules 1999;32:1260–3.
[44] Fujishige S, Kubota K, Ando I. J Phys Chem 1989;93:3311–3.
[45] Zheng YJ, Merz KM. J Comput Chem 1992;13:1151–69.
[46] Tamai Y, Tanaka H, Nakanishi K. Macromolecules 1996;29:6750–60.
[47] Cho EC, Lee J, Cho K. Macromolecules 2003;36:9929–34.